



Impact of cellulose nanofibers on cellulose acetate membrane performance

Gabriela A. Bastida · Roberto J. Aguado ·
María V. Galván · Miguel Á. Zanuttini ·
Marc Delgado-Aguilar · Quim Tarrés

Received: 6 October 2023 / Accepted: 16 January 2024 / Published online: 5 February 2024
© The Author(s) 2024

Abstract Membranes find applications across a wide spectrum of industries, including water treatment, energy production, and biomedicine. In this study, nonwoven membranes were fabricated using cellulose acetate (CA) as the primary component, with varying percentages of cellulose nanofibers (CNFs) embedded as reinforcement. These CNFs were prepared through an oxalic acid pretreatment (Oxalic-CNFs). Their incorporation into electrospun membranes represents an innovative approach, enhancing their mechanical properties for applications subjected to high loads and improving its functionalization capabilities. The impact of Oxalic-CNFs on membrane properties was investigated at nanofiber loadings ranging from 0 to 18 wt%. Membranes produced with 6 wt% Oxalic-CNF exhibited the superior physical and mechanical properties.

This improvement can be attributed to the formation of threads with higher intrinsic strength, a reduction in pore size, and an increase in density. When higher percentages of CNFs were added, the membranes were not properly formed, because filaments were not continuous and the needle became clogged. The substructure of the membrane proved to be a critical factor for mechanical properties, with remarkable increases in tensile strength and elastic modulus (around 300%) when comparing 4–6 wt% Oxalic-CNF-loaded membranes to CA membranes.

Keywords Membranes · Electrospinning · Cellulose nanofiber · Cellulose acetate · Oxalic acid

Supplementary Information The online version contains supplementary material available at <https://doi.org/10.1007/s10570-024-05760-9>.

G. A. Bastida · R. J. Aguado (✉) · M. Delgado-Aguilar · Q. Tarrés
LEPAMAP-PRODIS Research Group, University of Girona, C/Maria Aurèlia Capmany, 61, 17003 Girona, Spain
e-mail: roberto.aguado@udg.edu

G. A. Bastida · M. V. Galván · M. Á. Zanuttini
Institute of Cellulosic Technology, Faculty of Chemical Engineering (FIQ-CONICET), National University of the Litoral, Santiago del Estero 2654, S3000AOJ Santa Fe, Argentina

Introduction

Investigating production methods, functionalization, and ways to improve membranes is crucial for several reasons. Membranes play a vital role in various industries, including water treatment, energy production, and biomedical applications (Shanbhag et al. 2007; Wang et al. 2019; Abdellah Ali et al. 2020). Membrane science has gained widespread recognition and adoption owing to its exceptional characteristics, such as ease of handling and low operational costs, making it an exceptionally efficient and environmentally friendly solution. At its core, membrane technology serves the fundamental purpose of separating diverse mixtures by selectively allowing the

passage of certain species while hindering others. This pivotal function finds application across numerous industries and underscores the significance of membrane research and development in modern science and engineering (Vatanpour et al. 2022). These membranes are primarily manufactured from various synthetic plastics, polyethersulfone (PES), polypropylene (PP), polyethylene (PE), polyvinyl alcohol (PVA), polyvinylidene fluoride (PVDF), and polysulfone (PSF). Additionally, there are membranes made from carbohydrate polymers such as cellulose acetate (CA) and chitosan (CS), among other materials (Chang et al. 2022; Zou and Lee 2022; Ma et al. 2023). At present, the predominant research thrust is centered on the utilization of biodegradable polymers and the enhancement of their performance. This concerted effort has the potential to usher in the development of environmentally friendly membranes, heightened process efficiency, cost-effective solutions, and enhanced product quality.

Polymer membranes can be manufactured through a variety of methods, such as phase inversion, stretching, track etching, sintering, and applying surface coatings onto a support substrate (Kumar et al. 2023). One effective method for producing membranes characterized by an exceptional area-to-volume ratio involves the utilization of electrospinning. This technique facilitates the creation of ultrafine fibers, typically measuring in the nanometer range, yielding a highly porous structure with an expansive surface area (Ma et al. 2005; Agrahari et al. 2017). This augmented surface area greatly bolsters the membrane's overall performance and its capacity to effectively separate and filter various substances (Duman et al. 2022; Russo et al. 2022). Consequently, it finds widespread utility in diverse fields, including biomedical applications (Li et al. 2002; Yan et al. 2022), and the development of sensitive sensors (Kim et al. 2006; Yang et al. 2022).

Cellulose acetate (CA), especially in membrane form via the electrospinning technique, offers considerable promise due to its exceptional properties that make it highly versatile for a wide range of applications. Depending on the degree of substitution, CA is a biodegradable polymer of amphiphilic or hydrophobic nature. Its membranes are commonly used in water treatment processes (Vatanpour et al. 2023),

pharmaceutical industry (Khoshnevisan et al. 2018), food production (Wongsasulak et al. 2010), and filtration (Zhou et al. 2016). In addition, CA is derived from natural cellulose, making it biocompatible and safe for use in biomedical applications (Ali et al. 2019). It is often used in the manufacture of medical devices, such as dialysis membranes, owing to its capacity to allow selective transport of small molecules while retaining larger molecules. In terms of environmental benefits, CA membranes are considered more eco-friendliness compared to other synthetic membranes. They are biodegradable and can be derived from renewable sources, such as wood pulp or cotton (Cheng et al. 2010).

Nevertheless, the mechanical properties of CA membranes are undeniably low, as reported by (Zhijiang et al. 2016) with values of 1.56 ± 0.19 MPa. These mechanical properties can be significantly enhanced by incorporating another polymer. For instance, a blend nanofiber scaffold of Poly (hydroxybutyrate) (PHB) and CA improved this property to 7.86 ± 0.67 MPa (Zhijiang et al. 2016). Moreover, cellulose nanofibers (CNFs) are highly esteemed not only for their ability to improve mechanical strength but also because they provide exceptional properties. Battirolo et al. (2017) demonstrated the creation of asymmetric membranes based on CA and CNFs through solvent-free induced phase separation. This process led to a sponge-like morphology, increasing porosity and, consequently, enhancing membrane performance. The advantages of employing cellulose nanofibers as reinforcement agent are well-established. Meanwhile, (Higashi et al. 2020) incorporated 2,2,6,6-Tetramethylpiperidine-1-oxyl (TEMPO)-oxidized CNFs into a low concentration polyvinylpyrrolidone (PVP) solution to alter thixotropy and stabilize the filaments and prevent fragmentation during electrospinning. Particularly, Oxalic-CNFs exhibits adequate nanofibrillation performance, flexibility, a substantial aspect ratio, and easily controllable viscosity. It is noteworthy that the introduction of carboxylic groups into CNFs, as emphasized by (Bastida et al. 2022) results in a distinct surface charge. This feature opens up a wide array of potential applications for CNF-reinforced membranes.

However, CNFs have some inherent properties that make them challenging to directly process via

electrospinning, such as insolubility in common solvents. Such insolubility is due to its numerous –OH polar groups, which form extensive hydrogen bonds with other hydroxyl groups on adjacent chains (Pino-Ramos et al. 2017). This property severely limits the ability to create an homogeneous polymer solution required for electrospinning. Additionally, CNFs exhibit poor processability. They tend to aggregate or clump together and lack the chain entanglement required for producing continuous fibers during the electrospinning process. Aggregates can obstruct the spinning apparatus, disrupting filament formation. Moreover, the high viscosity of CNF suspensions presents challenges in achieving the appropriate flow rate and jet stability vital for a successful electrospinning process. Furthermore, as noted by (Chen et al. 2022), CNFs display a strong affinity for water, leading to rapid water absorption. This inherent hydrophilicity can result in CNFs losing their structural integrity and forming a gel-like system, rendering them unsuitable for electrospinning.

Therefore, in this work the impact of adding Oxalic-CNFs has been evaluated with the purpose of improving the performance of cellulose acetate membranes. Although various chemical treatments and different techniques have been explored to overcome its limitations, it remains a challenge at present along with getting proper electrospinning. For this, cellulose acetate membranes with different percentages of Oxalic-CNFs were obtained by electrospinning and were deeply characterized to determine their physical properties. Then, the structural and morphological properties of the membranes reinforced with Oxalic-CNFs were characterized by SEM (scanning electron microscopy). Thermo-plastic behavior of the membranes was verified by printing a mold on the film by hot-compression and mechanical properties also were evaluated. Finally, the presence of Oxalic-CNFs was verified by Fourier transform infrared spectroscopy (FTIR) and fluorescence. This study makes a significant contribution to the field of high-tech materials by introducing Oxalic-CNFs into AC membranes. These Oxalic-CNFs not only improve mechanical properties but also offer accessible carboxylate groups. The findings highlight the potential of functionalizing these Oxalic-CNFs, transforming them into an attractive system with numerous potential applications.

Experimental

Materials

Cellulose acetate (CA, 39.7% acetyl content, average $M_w=50,000$), acetone, N-dimethylformamide (DMF), oxalic acid, europium chloride, and 1,10-phenanthroline were purchased from Sigma-Aldrich, USA and used as received.

Cellulose nanofibers were prepared according to the method outlined by (Bastida et al. 2022). In brief, the starting material was bleached eucalyptus pulp (BEP) with a DPw of 7750 specified by the supplier, containing 69.8 ± 1.5 wt% cellulose, 26.50 ± 2.3 wt% hemicelluloses, 3.25 wt% lignin, 0.25 wt% extractives and 0.20 wt% ashes, provided by Suzano Papel e Celulose S.A. (Aracruz, Brazil). The pulp was initially subjected to treatment in a PFI mill refiner, undergoing 10,000 revolutions. Subsequently, a chemical pre-treatment with 50 wt% oxalic acid was conducted for 1 h at 90 °C. Finally, fibrillation was carried out using a high-pressure homogenizer, by 5 passes at 300 bar. In the second stage, nano-fraction was separated from the micro-fraction through centrifugation at 4800 G-force for 20 min.

Preparation of membranes

Electrospun CA membranes were prepared following the method outlined by (Chen et al. 2020). Typically, a 10 wt% CA homogeneous electrospinning solution was prepared in an improved ternary solvent system of acetone/DMF/water in a 3:2:1 ratio and stirred for 6 h at 25 °C as a reference. In literature has demonstrated that a mixed solvent system is more suitable than a single solvent, as it allows for the adjustment of polymer solution parameters such as surface tension and viscosity (Haas et al. 2010; Wsoo et al. 2020). Furthermore, the incorporation of water reduces the overall evaporation rate in the electrospinning air gap, providing sufficient time for fiber draw-down and reducing the likelihood of clogging at the spinneret (Frey 2008).

The membranes were prepared using an electrospinning setup (Fuidnatek, Bionicia, Paterna, Spain) equipped with a 20-gauge needle tip (Nominal outer diameter of the needle: 0.908 mm). The feed rate was set at $35 \mu\text{L min}^{-1}$, an applied voltage of 16 kV was employed, and the receiving distance between

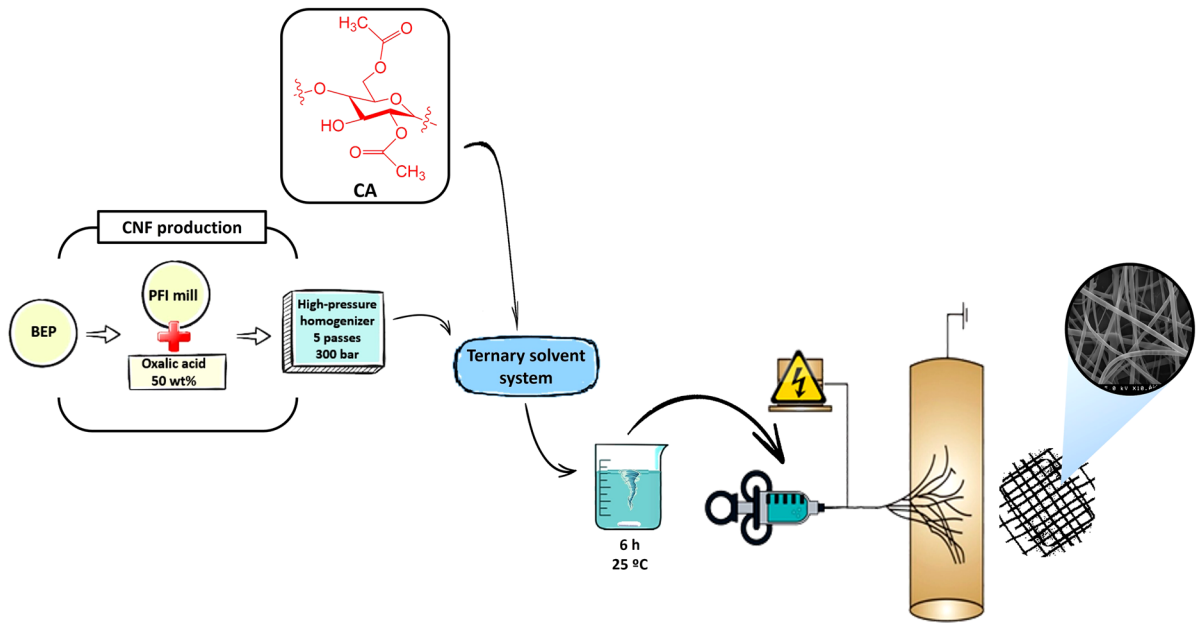


Fig. 1 Stage of membranes preparation process

the needle tip and aluminum foil collector was maintained at 5 cm. The resulting filaments were detached from the foil collector and air-dried. To produce Oxalic-CNFs/CA membranes, the volume of water was substituted with Oxalic-CNF suspensions at various concentrations. Figure 1 illustrates the flowchart of the membrane production process.

The designations of the membranes produced with different mass percentages of Oxalic-CNFs are listed in Table 1.

Characterization of Oxalic-CNFs and membranes

Nanofibrillation yield

The nanofibrillation yield was assessed by centrifuging an aqueous suspension containing 0.1 wt% Oxalic-CNFs at 2800 g for 20 min. The dry weight of the supernatant was determined as the difference between the initial weight (W_i) and the weight of the sediment obtained after centrifugation (W_p), using the following equation:

Table 1 Identification of membranes according to the Oxalic-CNF's percentage

Sample	CA (g)	Acetone (g)	DMF (g)	Water (g)	CNF (g)	Oxalic-CNFs (%)
M0	10	45	30	15	0.00	0.0
M1	9.98	45	30	15	0.02	0.2
M2	9.85	45	30	15	0.15	1.5
M3	9.7	45	30	15	0.30	3.0
M4	9.4	45	30	15	0.60	6.0
M5	8.8	45	30	15	1.20	12.0
M6	8.2	45	30	15	1.80	18.0

$$Yield(\%) = \left[\frac{W_i - W_f}{W_i} \right] * 100 \quad (1)$$

Cationic demand

Cationic demand (CD) was determined using a Müttek Particle Charge Detector PCD-06 from BTG Instruments (Weßling, Germany). In brief, 0.1 g of dry Oxalic-CNFs were mixed with a known excess of poly(diallyldimethylammonium chloride) (PDADMAC), typically 10 mL ($V_{PDADMAC}$), in a deionized water medium. The suspension was then subjected to centrifugation for 30 min at 3000 G-force. Subsequently, the supernatant was carefully decanted and titrated with sodium polyethylene sulfonate (PES-Na) until reaching the isoelectric point (0 mV). The cationic demand (CD) was calculated from:

$$CD = \frac{(C_{PDADMAC} * V_{PDADMAC}) - (C_{PES-Na} * V_{PES-Na})}{m} \quad (2)$$

where $C_{PDADMAC}$ is the normal concentration of PDADMAC (typically 0.001 N), C_{PES-Na} is the normal concentration of titrating agent (typically 0.001 N), m is the mass of sample, and V_{PES-Na} is the titration volume.

Transmission electron microscopy (TEM)

Transmission electron microscopy observations (JEOL, JEM-2100 Plus, Tokyo, Japan) were performed in HRTEM mode, with an accelerating voltage of 100 kV. A 0.001 wt% aliquot of Oxalic-CNF suspensions was mounted on a carbon-coated Cu grid.

The membranes were conditioned at a temperature of 23 ± 1 °C and a relative humidity of 50% for 48 h prior to testing. Each sample was analyzed in five replicates, and the results were subsequently averaged.

Physical properties

The grammage of membranes was determined by the ratio between the weight and surface. The thickness of the membranes was measured using a digital micrometer. Bendtsen surface roughness of the samples were measured using a Bendtsen tester (Metrotec, manufactured according to ISO 8791-2 standard).

Density of all prepared membranes was determined. The percentage of void volume, i.e. porosity, was also calculated from Eq. (3):

$$\text{Void volume (\%)} = 100 \cdot \left(1 - \frac{\rho_{\text{membrane}}}{\rho_{CA}} \right) \quad (3)$$

where ρ_{membrane} and ρ_{CA} are the different membranes and the cellulose acetate density, respectively. The transmittance of membranes was assessed using a UV–visible spectrophotometer (Lambda 35, Perkin-Elmer, Waltham, MA, USA) functioning within the wavelength interval of 400–800 nm. The spectra were recorded, with air serving as a reference for comparison.

Morphological analysis by electronic microscopy

To examine the morphological characteristics and dimensions of the as-spun materials, a scanning electron microscope (FE-SEM Hitachi S-4100, Japan) was employed. Images were captured using Quartz PCI software at accelerating voltages of 5 kV. To prepare the samples for analysis, they were affixed to a sample holder using a conductive carbon tape and subsequently coated with a thin layer of carbon through the evaporation method, employing an Emitech K950 turbo evaporator device from Germany.

Conductivity and rheological behavior

The electrical conductivities were measured at room temperature in a Metrohm 912 bench-top conductometer (Metrohm AG, Herisau, Switzerland). Rheological behavior was studied using a modular compact rheometer MCR 302e (Anton Paar, Graz, Austria).

Hot compression molding

To investigate the thermoplastic behavior of the membranes, hot compression molding at 90 °C was performed, similar to (Solier et al. 2022). In this test, a 3D-printed mold of PLA (50×30 mm²), with the LEPAMAP logo was employed for branding purposes. The membranes were placed on the mold, sandwiched between layers of blotting paper. Subsequently, pressure was applied using a hydraulic press equipped with preheated metallic plates. The entire

setup was maintained in an oven at 90 °C for 5 min. Following removal from the oven, the membranes were separated from the assembly. The thermal analyzes were carry out using a thermogravimetric analyzer (Mettler Toledo TGA/DSC1, Schwerzenbach, Switzerland), in a temperature range from 30 to 600 °C, at a heating rate of 10 K min⁻¹, under an inert nitrogen atmosphere and differential scanning calorimetry was performed with a (Mettler Toledo DSC822e, Columbus, OH, USA) from 25 to 100 °C with a resolution of 0.04 mW (at a heating rate of 6 K min⁻¹).

Contact angle

The surface hydrophobicity of the material was determined by measuring the static contact angle of water on membranes surfaces using a DSSA25 drop-shape analyzer from Krüss GmbH (Germany) with Krüss Advance Software. The measurements were performed at room temperature with a frequency of two measurements per second.

Mechanical properties

Tensile tests were carried out using INSTRON 3340 equipment with a 100 N cell. The measurements were performed on strips with 15 mm width and 80 mm length at a crosshead speed of 5 mm/min.

Fluorescent activity by dip coating

Europium chloride (EuCl₃·6H₂O), and 1,10-phenanthroline were taken in a 500 mL flask and 200 mL of ethanol/water solution (1:2 v/v) was added to it. The solution was stirred for 30 min. Membranes were immersed in 5 mL of solution for 5 min, washed with distilled water, and then dried under ambient conditions. The embedded membranes were analyzed for luminescence at room temperature. The excitation wavelength was fixed at 254 nm using a UV-lamp (25W with E26/E27 ozone socket, Stanley Electric GmbH, Moerfelden-Walldorf, Germany).

Fourier transform infrared analysis (FTIR)

The membranes with different percentages of Oxalic-CNFs were analyzed by FTIR. The carboxyl groups incorporated into the Oxalic-CNFs by treatment with

oxalic acid were identified using the Fourier transform infrared spectroscopy. Spectra were collected on a Bruker Alpha FT-IR spectrometer equipped with a diamond crystal plate ATR MIR single-reflection accessory, at a resolution of 4 cm⁻¹ from 500 to 3500 cm⁻¹. Each sample was scanned 25 times.

X-ray diffraction (DRX)

X-ray diffraction analysis was performed used a Bruker AXS diffractometer, model D8 Advance, with Cu-K α radiation (154 pm) and variable slits.

Results and discussion

Characterization of Oxalic-CNFs and membranes

In the context of incorporating Oxalic-CNFs into CA membranes, it is essential to begin with an understanding of the properties of the Oxalic-CNFs materials themselves. This initial characterization serves as a critical foundation for subsequent research. In this regard, our investigation revealed a nanofibrillation yield of 48.9% and a cationic demand of 72 $\mu\text{eq/g}$ Oxalic-CNFs. These values align closely with the findings reported in the previous study (Bastida et al. 2022).

Physical properties

In terms of the physical properties, Table 2 presents data on average thickness, grammage, and density. A slight increase, up to 6% Oxalic-CNFs added, is observed in these properties. However, beyond this threshold, there is a decline in the material's characteristics. This pattern is similarly reflected in the void volume, which is associated to porosity. As expected, a linear trend is evident for most cases studied, except for M5 and M6. Interestingly, these two membranes exhibit an increase in void volume. The behavior of these fibrous structures is intricately linked to the dimensions, configurations, and arrangement of the fibers within them. These factors collectively influence the properties of the interstitial spaces or gaps between the fibers. The density at which the fibers are packed together ultimately dictates the overall porosity of the fibrous membranes (Liu and Hsieh 2002). Moreover, the incorporation of Oxalic-CNFs has

Table 2 Physical properties of membranes with different percentage of Oxalic-CNFs

Sample	Thickness ^a (mm)	Grammage ^a (gsm)	Density ^a (g/cm ³)	Void volume (%)	Roughness ^a (mL/min)
M0	0.023 ± 0.007	15 ± 1	0.65 ± 0.07	49.28	47 ± 5
M1	0.027 ± 0.001	19 ± 1	0.65 ± 0.05	49.22	37 ± 6
M2	0.030 ± 0.010	22 ± 6	0.68 ± 0.05	46.72	75 ± 3
M3	0.043 ± 0.004	27 ± 2	0.75 ± 0.05	41.41	80 ± 1
M4	0.047 ± 0.004	39 ± 2	0.78 ± 0.03	39.06	95 ± 6
M5	0.041 ± 0.002	24 ± 2	0.66 ± 0.07	48.44	320 ± 20
590 M6	0.036 ± 0.006	26 ± 4	0.67 ± 0.04	47.66	590 ± 10

^aValues are the average of five replicates

been found to contribute to an increase in membrane roughness.

As reported by (Sharma et al. 2021), at low concentrations of CNFs, they interact through hydrogen bonding with CA, resulting in a homogeneous system. However, this study also noted that as the CNFs content increases, they tend to aggregate due to their higher affinity for each other, stemming from their elevated specific surface area and binding capacity. In this context, the formation of aggregates in samples M5 and M6 would explain the shift in physical properties such as density and porosity in terms of void space.

Figure 2 presents images of different membranes, offering a visual insight into their morphological characteristics and transparency, both of which are crucial indicators at the nanoscale level. Surprisingly, no discernible pattern emerges, and they are in agreement with the light transmittance results shown in

Fig. S1 of the Supplementary Material. This variation in appearance is likely attributed to the diverse filament arrangements within the membranes. The level of opacity or transparency in a membrane primarily hinges on its structural arrangement and chemical composition. Membranes with higher density typically exhibit a more tightly packed structure with fewer intermolecular spaces, resulting in reduced light transmission capabilities.

Morphological analysis by microscopy

In Fig. 3, SEM images reveal the surface characteristics of CA filaments. These filaments exhibit a smooth, continuous, and regular surface, similar aspect to that reported by (Golizadeh et al. 2019). When compared to pure CA, the addition of Oxalic-CNFs did not induce significant alterations in filament surface morphology. However, a notable reduction in



Fig. 2 Photographs of the membranes placed on a piece of paper. The paper used is also shown

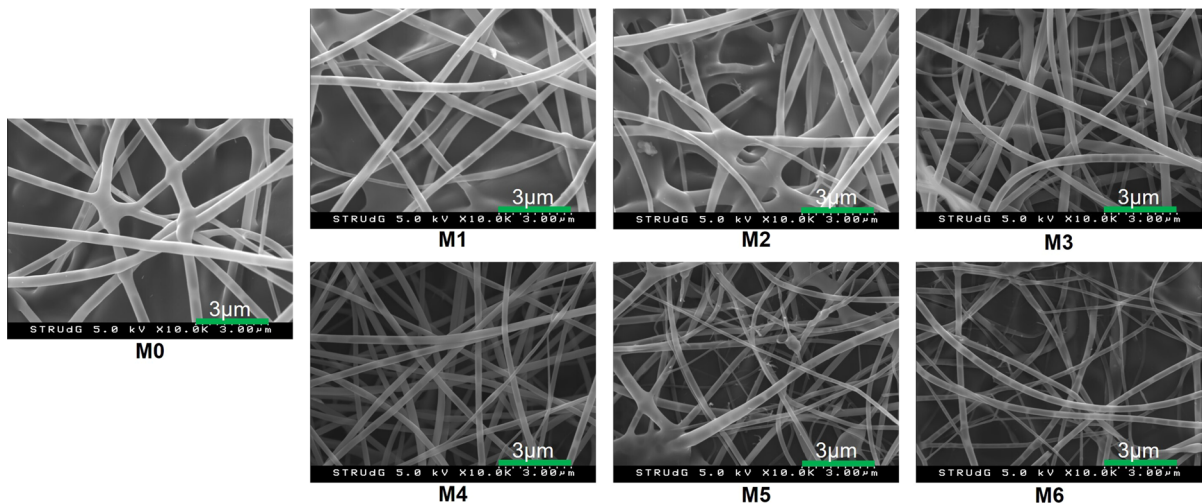


Fig. 3 SEM images of CA membrane as reference (M0), and membranes with different percentages of Oxalic-CNFs

filament diameter can be attributed to the presence of Oxalic-CNFs, despite the limitations of this technique in visualizing the distribution of nanofibers within the membranes.

In Fig. 4, the results illustrating the average filament diameter are presented. As previously discussed, the introduction of Oxalic-CNFs results in a notable reduction in filament diameter. Notably, Fig. 4h reveals an intriguing linear trend, defying expectations. Moreover, when it comes to fiber diameter, the solution viscosity is an important factor, particularly if there is no splitting. Higher viscosity leads to a larger diameter of the fiber and this phenomenon can likely be attributed to the increased resistance of the solution to stretching caused by the charges on the jet (Bera 2016). Nevertheless, we observe the behavior is exactly the opposite, decrease, similar to reported by (Higashi et al. 2020). These authors showed that, the average diameter of the filaments decreases from 98 to 92 nm, when 0.4 wt% of CNF-TEMPO is added. However, at 0.8 wt%, it increases again, reaching a value of 131.7 nm. Thus, this phenomenon can be attributed to a decrease in the flow rate value, as a result of the introduction of a greater percentage of insoluble particles characterized by a lower aspect ratio. This causes a reduction in the effective section of the jet and a decrease in the diameters of the filaments. A similar behavior was noted by (Aboamara et al. 2019), when they incorporated graphene oxide into cellulose acetate membranes by electrospinning.

It is imperative to examine the viscosity and conductivity of the solutions to be electrospun, as these variables play essential roles in the formation of electrospun fibers. As expected, the conductivity of the solutions increased proportionally with the addition of Oxalic-CNFs (Fig. 5a). Oxalic-CNFs with 1 wt% concentration exhibited a relatively high conductivity (67.8 $\mu\text{S}/\text{cm}$), which may explain the marked influence it has on the current flow. In general, it is noticed that when the solution has a higher conductivity, the filaments formed during electrospinning have a smaller diameter. This is because of a more efficient charge transfer through the solution being electrospun. The conductivity of the solution helps in distributing the electrical charge more uniformly, which ultimately influences the creation of the Taylor cone at the needle's tip during the electrospinning process (Xue et al. 2019; Morais et al. 2022).

Regarding the rheological behavior, Fig. 5b shows the cutting speed versus the shear stress for the solutions studied at two different temperatures (20 and 40 °C). Newtonian behavior was observed for all systems, even in the presence of Oxalic-CNFs. Furthermore, the increase in viscosity observed in the solution with 18 wt% Oxalic-CNFs explains the poor spinnability observed. While adding 6 wt% of Oxalic-CNFs, viscosity was similar to that of CA in the ternary solvent. The effect of temperature is also a factor to consider due to the high voltage used and the subsequent dissipated energy. Even at 40 °C,

the behavior is repeated and the solution containing 18 wt% of Oxalic-CNFs is the most viscous.

Figure 6a shows the M4 membrane after the hot compression molding process and images of all formulations can be found in Fig. S2 in the Supplementary Material. As expected, these membranes effectively retained the thermoformability inherent to CA. Due to the presence of Oxalic-CNFs network, the replication of intricate mold details became feasible. It is worth reiterating that these membranes exhibit dissimilar appearances, but the hot compression molding process left the color, transparency, and homogeneity of the membrane unchanged. The thermal analyses (Figs. S3 and S4 of the Supplementary Material) show, on the one hand, two thermal processes that the membranes undergo, corresponding to the volatilization of the absorbed residual water (~190 °C) and the degradation of the CA chains (~360 °C), without appreciable differences between them. On the other hand, up to 100 °C, DSC analysis does not reveal any transition apart from the water desorption that takes place at 30 °C. Therefore, the choice of temperature to perform hot compression molding is justified, since at 90 °C no degradation of the membranes is seen. These findings indicate that the addition of Oxalic-CNFs to cellulose membranes improves their properties without altering their thermal behavior. Furthermore, in Fig. 6b, the produced filaments have a length greater than 90 µm. These filaments appear disordered and exhibit a superficially smooth texture. During the jet stretching process, the solution successfully sustained continuous extension, leading to the formation of long, beaded fibers or fused fibers.

Contact angle

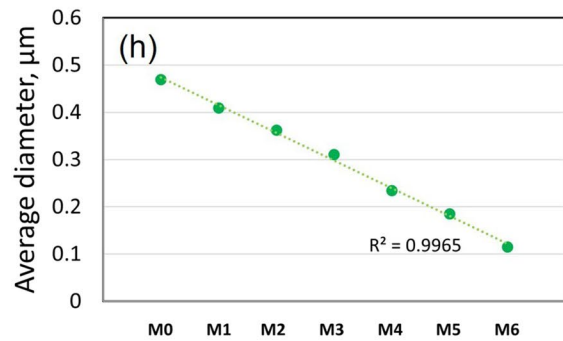
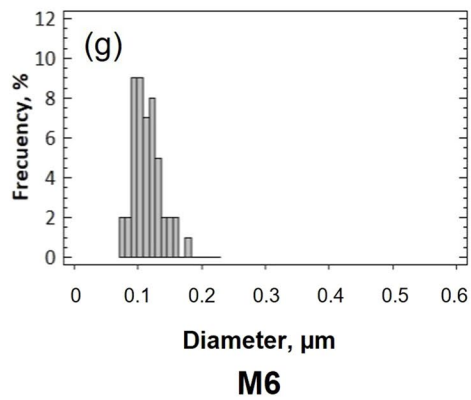
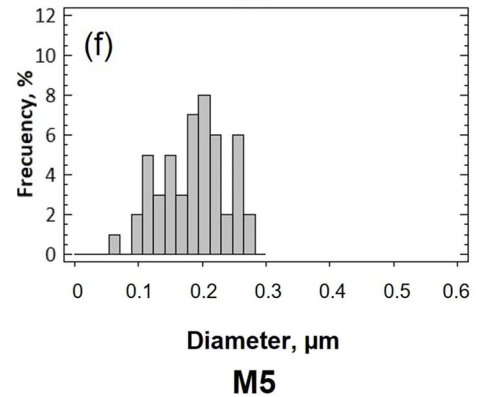
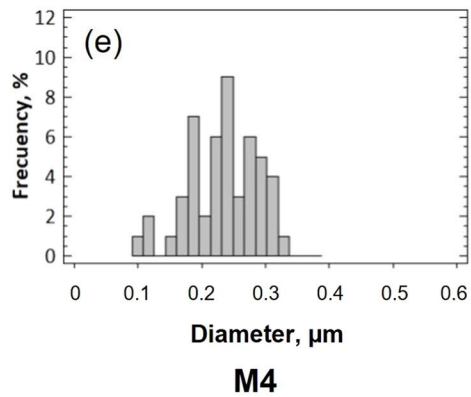
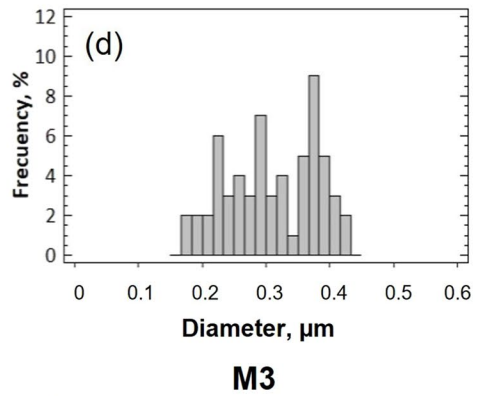
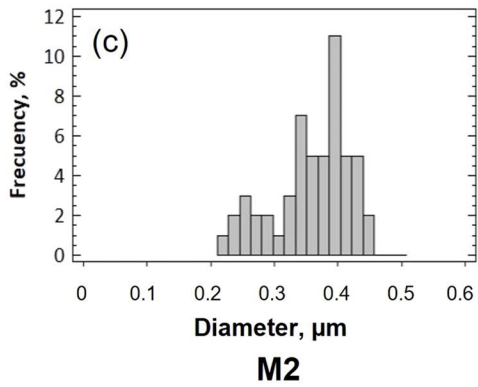
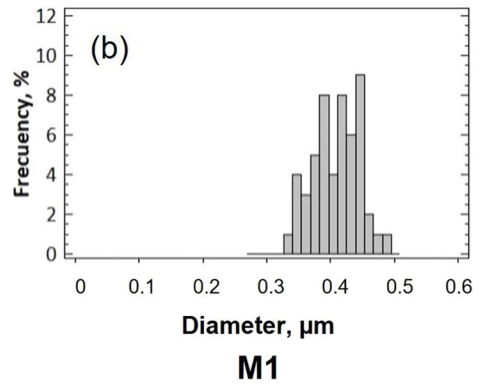
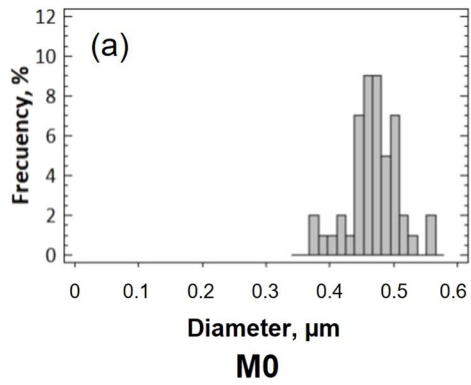
The hydrophilicity of the top membrane surfaces was evaluated by measuring the water contact angle (Table 3). The surface of the reference M0 presents a value of 43.4°. CA presented a typical hydrophilic surface contact angle value similar to that reported by (Battirolo et al. 2017) for CA membranes prepared by non-solvent phase inversion process. CA scaffolds prepared by electrospinning revealed equally hydrophilic surfaces, (Zhijiang et al. 2016) obtained an approximate contact angle of 70°. Regarding to the addition of Oxalic-CNFs to the CA matrix increased the contact angle. Particularly, the addition of 6 wt % of Oxalic-CNFs shows the highest contact angle

value (59.9°) indicating that the capacity to resist water is increased; namely, the hydrophobic performance of the surface was enhanced. Nonetheless, no noteworthy distinctions in the values were discernible across various Oxalic-CNF percentages. The contact angle appears to have a strong correlation with porosity, primarily owing to capillarity phenomena (Drelich et al. 2020). This suggests that CNF presence generates filaments with smaller diameters and thus results in a membrane with higher compactness. Furthermore, surface curvature could potentially play a role in the observed contact angles.

Mechanical properties

Figure 7a illustrates the tensile strength of various membranes, including the reference (M0), and samples with different percentages of Oxalic-CNFs. In the case of M0, a value of 3.3 ± 0.1 MPa was obtained. The mechanical properties of the CA membranes were studied by (Golizadeh et al. 2019), where they reported a tensile strength of approximately 2.5 MPa. The authors explained that the low tensile strength of electrospun nanofiber mats was a result of loosely packed fibers and a low degree of cross-linking between fibers. Fortunately, our results show a significant increase ($p < 0.05$) in tensile strength when Oxalic-CNFs were incorporated. Even a small addition of CNF noticeably improves performance, and several authors attribute this behavior to the intrinsic tensile qualities of the reinforcement (Tarrés et al. 2020; Singh et al. 2022).

An improvement of 383% was achieved with the addition of 6 wt% Oxalic-CNFs, which can be attributed to the high aspect ratio and strong mechanical strength of CNFs, as well as the robust interactions between CNFs and CA (Peng et al. 2011). Additionally, Oxalic-CNFs are flexible due to their aspect ratio, suggesting a propensity to entangle under static conditions (Bastida et al. 2023). Notably, when a higher percentage of Oxalic-CNFs was incorporated, proper electrospinning was not achieved. This was likely due to system obstructions, filament discontinuity, and slow solvent evaporation. Despite maintaining consistent electrospinning parameters, it was not possible to produce the porous and nanocrosslinked expected membranes, resulting instead in a dense and non-homogenous mat, as shown in Fig. 7b. This can be explained because the viscosity,



◀**Fig. 4** Distribution of diameter **a–g** to 18 wt% of Oxalic-CNFs and linear trend of average diameters **h** of membranes with different Oxalic-CNF's percentage

as mentioned before, is higher and impairs spinnability. Additionally, SEM images of the membrane with different magnifications are shown in Fig. S5 of the Supplementary Material. In them it is possible to observe the formation of aggregates that takes place when a percentage of Oxalic-CNFs greater than 6 wt% is added.

A similar increasing trend was observed in the strain membranes as a consequence of increasing content of Oxalic-CNFs, as depicted in Fig. 8a. The results indicate that Oxalic-CNFs are well-dispersed on the filaments and can form new hydrogen bonds, thereby enhancing tensile properties. Additionally, the uniform dispersion of nanofibers aids in mitigating premature fracture caused by stress concentration arising from the existence of clusters (He et al. 2023) which is in line with the simultaneous increase in maximum stress and strain at break. Although M4 exhibits the best maximum strain value, the percentage of Oxalic-CNFs does not have a significant effect ($p > 0.05$) on this property. Furthermore, beyond a certain concentration of Oxalic-CNFs, aggregates can form leading to no further improvement in mechanical strength. These findings align with those investigated by (Schnell et al. 2023) in xylan/chitosan films when CNFs are introduced. In a similar context, several authors have noted that the size distribution is directly correlated with mechanical properties. CNFs with larger sizes are expected to be more flexible, but they are prone to tangling, causing dispersion issues in the polymer solution as the quantity increases (Lu et al. 2017; Li et al. 2022). Fracture stress–strain curves for each membrane can be seen in the Supplementary Material (Fig. S6).

The Young's Modulus (YM) of the membranes as a function of Oxalic-CNF content is presented in Fig. 8b. Initially, the reference membrane exhibits a YM of 176 ± 15 MPa, which is comparable to values reported in other studies. (Golizadeh et al. 2019) reported a value of approximately 125 MPa, while (Thomas et al. 2022) obtained a YM of 120 MPa. Furthermore, it is known that other authors have reported values lower than 20 MPa (Baek et al. 2011; Sinha et al. 2020) due to the weak mechanical resistance of pristine electrospun CA membranes. This

limitation motivated them to explore various strategies to enhance their mechanical properties. In our case, the addition of different percentages of Oxalic-CNFs allowed us to consistently increase the YM. The maximum value of 580 ± 13 MPa was achieved with 18% Oxalic-CNFs. Since Oxalic-CNFs have a high aspect ratio, they impart significant stiffness. As mentioned by (Benítez and Walther 2017), it is crucial to consider that the stiffness of CNFs is influenced by the proportion of crystalline and amorphous domains within them, which, in turn, is determined by the source of the nanofibrils and their treatment. Furthermore, the authors explain that during the initial alignment in the tensile test, porosity decreases, resulting in a mechanically more cohesive fibrillar network with greater rigidity, resistance, and reduced elongation. This observed rise in YM with increasing amount of Oxalic-CNFs in the membranes confirms successful dispersion and distribution of the reinforcement phase.

Fluorescent activity by dip coating

The presence of Oxalic-CNFs becomes evident upon exposure to ultraviolet (UV) light. As depicted in Fig. 9a, a red color emerges as a result of a chemical reaction between the carboxylate groups present in Oxalic-CNFs and EuCl_3 . This reaction leads to the formation of a red complex that becomes visible when subjected to UV light. The presence of Europium (Eu) in EuCl_3 is of particular significance due to its unique electronic configuration, allowing it to emit red light when excited by a specific UV light wavelength, as documented by (Aguado et al. 2023). It is worth noting that the formation of this complex and the observation of the red color under UV light are contingent on the availability of carboxylate groups as well as the concentration and nature of the reagents employed. The chromophore ligand, 1,10-phenanthroline, serves as a photon antenna absorbing light and efficiently transferring excitation energy to the Eu(III) ion, as elucidated by (Pavithran et al. 2005). Consequently, the intense and characteristic fluorescence of the Eu(III) ions becomes evident. The interaction between the carboxylate groups of Oxalic-CNFs and EuCl_3 is illustrated in Fig. 9b. Successfully, dip coating reveals that Oxalic-CNFs are accessible on the membranes. Otherwise, the complex would not have formed.

Fig. 5 **a** Conductivity and **b** rheological behavior of CA solution and CA with 6 and 18 wt% of Oxalic-CNFs at 20 and 40 °C

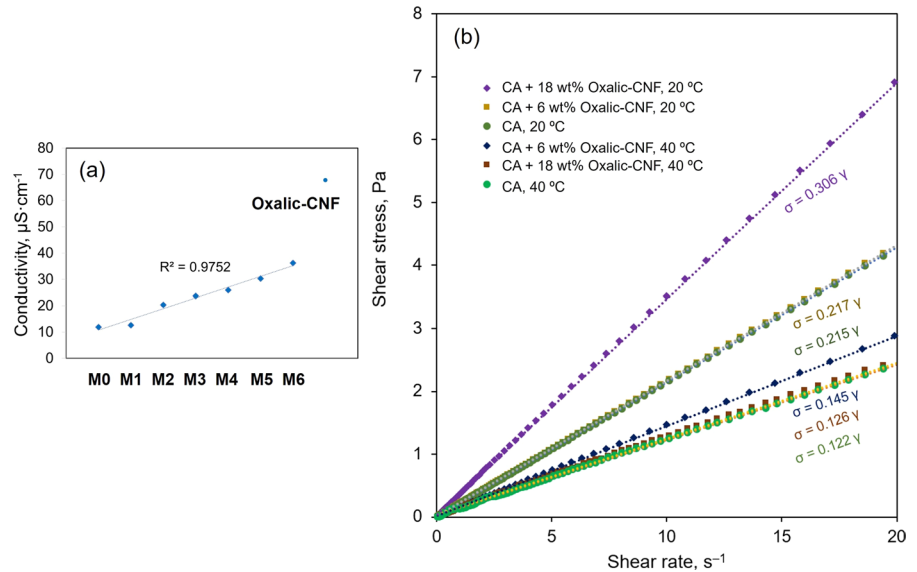
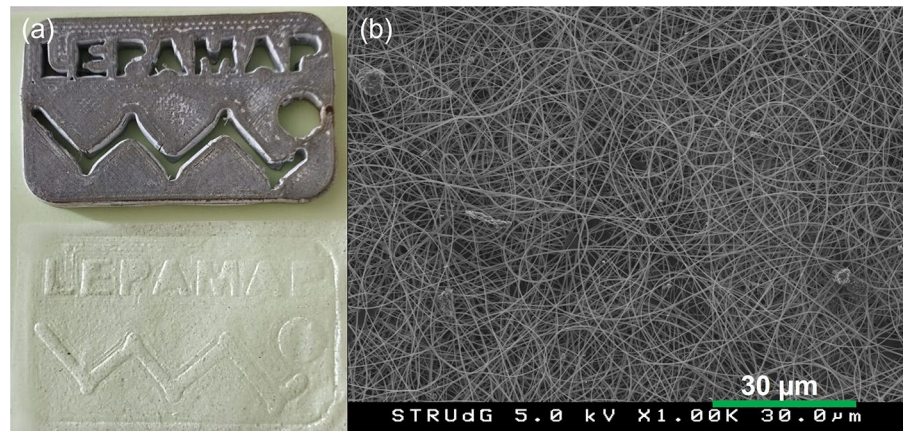


Fig. 6 **a** Hot compression molding and **b** SEM image of M4 membrane. The mold used to mark that the film is also shown



Fourier transform infrared analysis (FTIR)

FTIR spectra of the membranes are presented in Fig. 10. The spectra reveal distinctive peaks associated with various chemical components. Specifically, the samples exhibit characteristic peaks of CA at 1240 cm^{-1} (corresponding to the C–O stretching of the acetyl group), 1375 cm^{-1} (C–H) related to bending vibrations of CH_3 in the acetyl group, and 1750 cm^{-1} indicative of the C=O stretching of the acetyl group as reported by (Fei et al. 2017). Furthermore, the cellulose present in the samples exhibits a distinct peak at 2898 cm^{-1} , attributed to the symmetric stretching vibration of C–H (Tripathi et al. 2017; Luo et al. 2019). Additionally, the

peak at 899 cm^{-1} can be assigned to the glycosidic linkages within the glucose ring of cellulose (Gañán et al. 2004). Notably, in all Oxalic-CNFs/CA membranes, a new and relatively weak peak at 1735 cm^{-1} is observed. This peak corresponds to vibrational stretching, as discussed by (Tripathi et al. 2017). Interestingly, this peak is absent in M0 (the reference sample) and becomes more pronounced with an increasing percentage of Oxalic-CNFs added. This phenomenon can be attributed to a chemical reaction between the hydroxyl group on the cellulose chains and the carboxyl group of oxalic acid. This reaction involves Fischer–Speier esterification of one carboxyl group of oxalic acid, a process that originates during the chemical

Table 3 Static water contact angle of membranes with different contents of Oxalic-CNFs

Sample	Contact angle (°) ^a	
M0	43.43 ± 1.26	
M1	43.32 ± 7.66	
M2	65.72 ± 1.47	
M3	58.70 ± 1.47	
M4	59.14 ± 7.31	
M5	53.58 ± 0.81	
M6	54.95 ± 0.98	

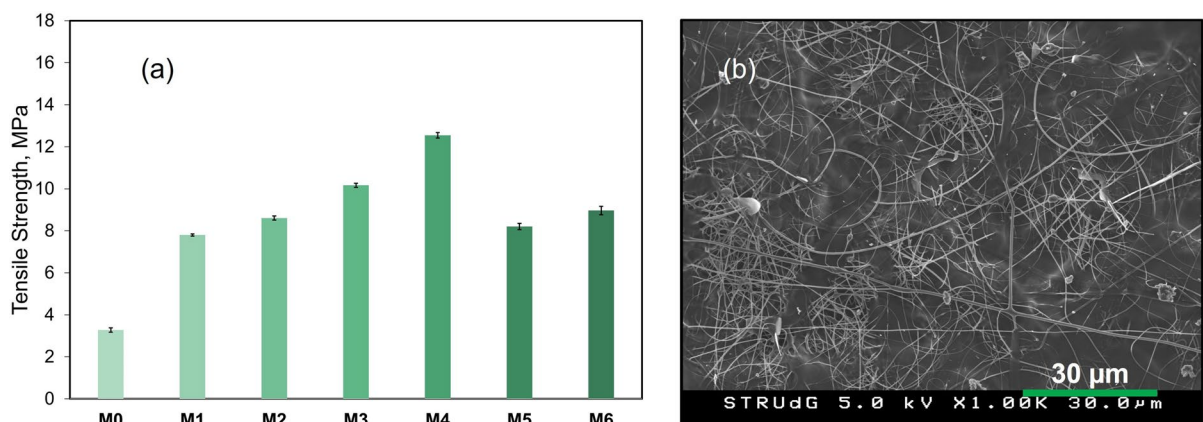
^aValues are the average of five replicates

pre-treatment in the production of the Oxalic-CNFs (Fig. S7 of the Supplementary Material).

X-ray diffraction (XRD) and transmission electron microscopy (TEM)

Based on the XRD patterns shown in Fig. 11a, there are two apparent broad peaks observed for CA. The one at low Bragg angles is assigned to different diffraction peaks at $2\theta \sim 8^\circ$ and 10° , while that at 20° has been associated with amorphous regions (Das et al. 2014). In contrast, the profile of Oxalic-CNFs was typical for highly crystalline nanocellulose, with its prominent (200) peak at $2\theta = 22.5^\circ$ and its (1–10)/(110) peaks between 15.1° and 16.3° (Barbosa et al. 2022). In the case of Oxalic-CNF-loaded membranes, the relative intensity of the so-called amorphous peak of CA decreased and the (200) peak of Oxalic-CNFs was not appreciated. It can be hypothesized that Oxalic-CNFs approach CA chains by the axial planes of the former, while their hydroxyl groups and their few carboxyl groups remain solvated by water, and this produces a particular rearrangement of the crystallites. On the other hand, the TEM image (Fig. 11b) suggests a good aspect ratio, uniform diameters (12 ± 3 nm), and a not too rigid morphology. These characteristics benefit dispersion, interaction, distribution in the filaments and do not generate high discontinuity in electrospinning.

The luminescence, FTIR and XRD analyses have yielded results indicating the presence of readily accessible Oxalic-CNFs within membranes. This

**Fig. 7** **a** Tensile Strength of membranes with different percentage of Oxalic-CNFs and **b** SEM image of M5. Values are the average of five replicates

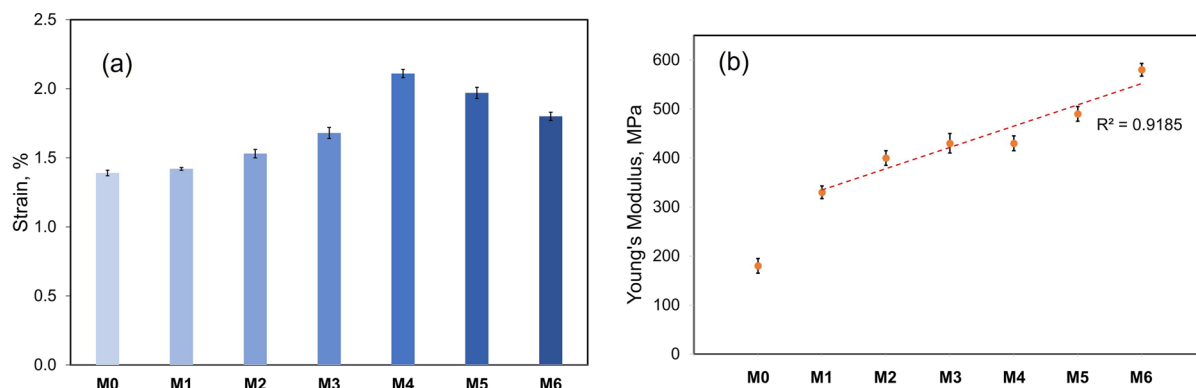
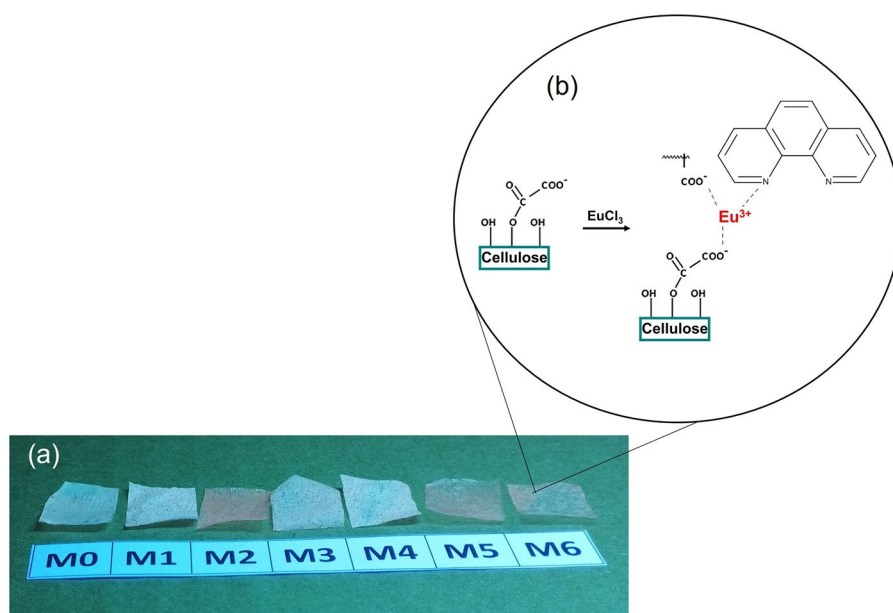


Fig. 8 Strain of membranes containing increasing amounts of Oxalic-CNFs. Values are the average of five replicates

Fig. 9 Luminescence of membranes with different Oxalic-CNFs percentage as result of the Eu(III) emission of red light



discovery opens exciting prospects for potential applications of these materials. Through the process of functionalization, specific chemical groups that imbue Oxalic-CNFs with distinct and desirable properties can be introduced, enhancing their utility and versatility.

Conclusions

Cellulose nanofiber reinforcement has been successfully incorporated into cellulose acetate membranes, yielding remarkable enhancements. This improvement strategy involved the strategic substitution of

a portion of the ternary solvent system, corresponding to water, acetone, and DMF, with an Oxalic-CNF solution. Compared to the CA reference membranes, the addition of Oxalic-CNFs (at concentrations ranging from 0.2 to 6% by weight) yielded materials with significantly enhanced mechanical strength. Notably, Oxalic-CNFs contributed to an impressive 383% increase in tensile strength, primarily attributed to the higher Oxalic-CNF content, resulting in a greater surface area and an increased number of inter-fiber bonds.

The introduction of Oxalic-CNFs was found to facilitate uniform distribution throughout the filament volume, promoting molecular-level contact during the

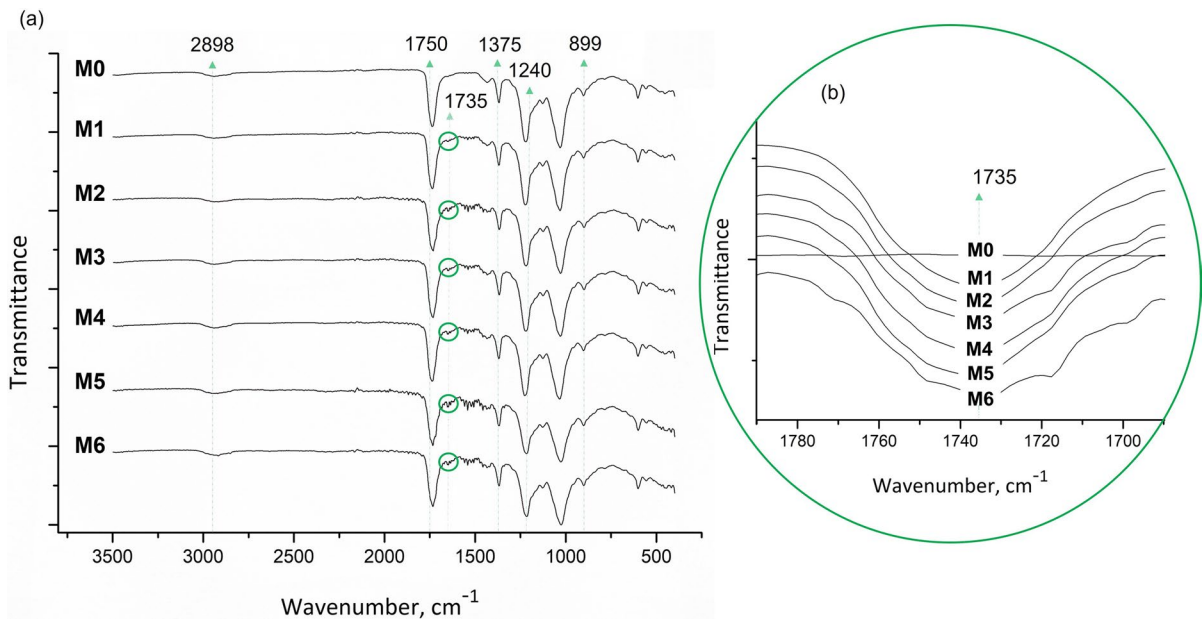
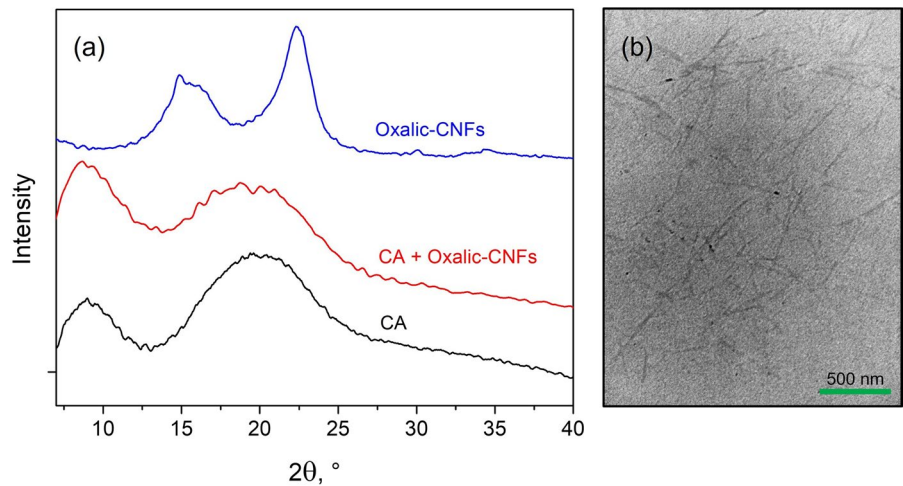


Fig. 10 FTIR spectra of the reference (M0) and membranes with different percentage of Oxalic-CNFs

Fig. 11 **a** XRD spectra of the Oxalic-CNFs, CA, and Oxalic-CNFs/CA and **b** TEM image of Oxalic-CNFs



drying process and effectively filling the pores, confirming good interfacial compatibility. This, in turn, led to the observed strength improvements. Additionally, FTIR spectra confirmed the presence of the Oxalic-CNFs carboxylate groups, further corroborating their incorporation into the CA membranes. Furthermore, when the membranes were immersed in a EuCl_3 solution and examined under ultraviolet light.

Besides, the fact that the membranes have been immersed in EuCl_3 solution and when observed with ultraviolet light the red color appears, reveals

that the Oxalic-CNFs are accessible. The valuable findings provide the opportunity to functionalize these membranes and provide them with unique characteristics.

Acknowledgments Authors wish to acknowledge the financial support of the funding agencies listed in the “Funding” section.

Authors’ information Marc Delgado-Aguilar and Quim Tarés are Serra Hunter Fellows.

Authors' contributions All authors contributed to the study conception and design. Material preparation, data collection and analysis were performed by Gabriela A. Bastida, Roberto J. Aguado and Quim Tarrés. The first draft of the manuscript was written by Gabriela A. Bastida and Roberto J. Aguado, and all authors commented on previous versions of the manuscript. María Verónica Galván, Miguel Á. Zanuttini, and Marc Delgado-Aguilar compiled all comments and prepared the final version of the manuscript, which was read and approved by all the authors.

Funding Open Access funding provided thanks to the CRUE-CSIC agreement with Springer Nature. This research was funded by the Spanish Ministry of Science and Innovation, project NextPack (PID2021-124766OA-I00).

Data availability Raw data of the present work can be made available upon request.

Declarations

Competing interests Authors declare that they have no known competing interests or personal relationships that could have appeared to influence the work reported in this paper.

Ethics approval and consent to participate Authors declare that the manuscript is not submitted to any other journal at the time of submission for simultaneous consideration, that the submitted work is original and has not been published elsewhere in any form, that this work is not part of a single study, that results are presented under the principles of honesty, without fabrication, falsification or inappropriate data manipulation, and that no data, text or theories by others are presented as our own.

Consent for publication All authors have revised the last version of the submitted manuscript, and we approve its submission.

Open Access This article is licensed under a Creative Commons Attribution 4.0 International License, which permits use, sharing, adaptation, distribution and reproduction in any medium or format, as long as you give appropriate credit to the original author(s) and the source, provide a link to the Creative Commons licence, and indicate if changes were made. The images or other third party material in this article are included in the article's Creative Commons licence, unless indicated otherwise in a credit line to the material. If material is not included in the article's Creative Commons licence and your intended use is not permitted by statutory regulation or exceeds the permitted use, you will need to obtain permission directly from the copyright holder. To view a copy of this licence, visit <http://creativecommons.org/licenses/by/4.0/>.

References

- Abdellah Ali SF, William LA, Fadi EA (2020) Cellulose acetate, cellulose acetate propionate and cellulose acetate butyrate membranes for water desalination applications. *Cellulose* 27:9525–9543. <https://doi.org/10.1007/s10570-020-03434-w>
- Aboamera NM, Mohamed A, Salama A, Khattab A (2019) Characterization and mechanical properties of electrospun cellulose acetate/graphene oxide composite nanofibers. *Mech Adv Mater Struct* 26:765–769. <https://doi.org/10.1080/15376494.2017.1410914>
- Agrahari V, Agrahari V, Meng J, Mitra AK (2017) Electrospun nanofibers in drug delivery: fabrication, advances, and biomedical applications. In: *Emerging nanotechnologies for diagnostics, drug delivery and medical devices*. Elsevier Inc., pp 189–215
- Aguado RJ, Gomes BO, Durães L, Valente AJM (2023) Luminescent papers with asymmetric complexes of Eu(III) and Tb(III) in polymeric matrices and suggested combinations for color tuning. *Molecules*. <https://doi.org/10.3390/molecules28166164>
- Ali ASM, El-Aassar MR, Hashem FS, Moussa NA (2019) Surface modified of cellulose acetate electrospun nanofibers by polyaniline/ β -cyclodextrin composite for removal of cationic dye from aqueous medium. *Fibers Polym* 20:2057–2069. <https://doi.org/10.1007/s12221-019-9162-y>
- Bastida GA, Schnell CN, Mocchiutti P et al (2022) Effect of oxalic acid concentration and different mechanical pre-treatments on the production of cellulose micro/nanofibers. *Nanomaterials*. <https://doi.org/10.3390/nano12172908>
- Bastida GA, Tarrés Q, Aguado R et al (2023) Flocculation of cellulose microfibril and nanofibril induced by chitosan-xylan complexes. *Nanomaterials*. <https://doi.org/10.3390/nano13172420>
- Battirolo LC, Andrade PF, Marson GV et al (2017) Cellulose acetate/cellulose nanofiber membranes for whey and fruit juice microfiltration. *Cellulose* 24:5593–5604. <https://doi.org/10.1007/s10570-017-1510-8>
- Benítez AJ, Walther A (2017) Cellulose nanofibril nanopapers and bioinspired nanocomposites: a review to understand the mechanical property space. *J Mater Chem A Mater* 5:16003–16024
- Bera B (2016) Literature review on electrospinning process (a fascinating fiber fabrication technique). *Imp J Interdiscip Res (IJIR)* 2:972–984
- Chang CC, Yu ST, Su JF, Cheng LP (2022) Asymmetric and bi-continuously structured polyethersulfone (PES) membranes with superior water flux for ultrafiltration application. *J Polym Res*. <https://doi.org/10.1007/s10965-021-02867-6>
- Chen W, Ma H, Xing B (2020) Electrospinning of multifunctional cellulose acetate membrane and its adsorption properties for ionic dyes. *Int J Biol Macromol* 158:1342–1351. <https://doi.org/10.1016/j.ijbiomac.2020.04.249>
- Chen P, Wohlert J, Berglund L, Furó I (2022) Water as an intrinsic structural element in cellulose fibril aggregates. *J Phys Chem Lett* 13:5424–5430. <https://doi.org/10.1021/acs.jpcclett.2c00781>
- Cheng HN, Dowd MK, Selling GW, Biswas A (2010) Synthesis of cellulose acetate from cotton byproducts. *Carbohydr Polym* 80:449–452. <https://doi.org/10.1016/j.carbpol.2009.11.048>

- da Barbosa RFS, Zanini NC, Mulinari DR, dos Rosa DS (2022) Hexavalent chromium sorption by modified cellulose macro and nanofibers obtained from eucalyptus residues. *J Polym Environ* 30:3852–3864. <https://doi.org/10.1007/s10924-022-02469-3>
- Das AM, Ali AA, Hazarika MP (2014) Synthesis and characterization of cellulose acetate from rice husk: eco-friendly condition. *Carbohydr Polym* 112:342–349. <https://doi.org/10.1016/j.carbpol.2014.06.006>
- Drelich JW, Boinovich L, Chibowski E et al (2020) Contact angles: history of over 200 years of open questions. *Surf Innov* 8:3–27
- Duman O, Uğurlu H, Diker CÖ, Tunç S (2022) Fabrication of highly hydrophobic or superhydrophobic electrospun PVA and agar/PVA membrane materials for efficient and selective oil/water separation. *J Environ Chem Eng*. <https://doi.org/10.1016/j.jece.2022.107405>
- Fei P, Liao L, Cheng B, Song J (2017) Quantitative analysis of cellulose acetate with a high degree of substitution by FTIR and its application. *Anal Methods* 9:6194–6201. <https://doi.org/10.1039/c7ay02165h>
- Frey MW (2008) Electrospinning cellulose and cellulose derivatives. *Polym Rev* 48:378–391. <https://doi.org/10.1080/15583720802022281>
- Gañán P, Cruz J, Garbizu S et al (2004) Stem and bunch banana fibers from cultivation wastes: effect of treatments on physico-chemical behavior. *J Appl Polym Sci* 94:1489–1495. <https://doi.org/10.1002/app.21061>
- Golizadeh M, Karimi A, Gandomi-Ravandi S et al (2019) Evaluation of cellular attachment and proliferation on different surface charged functional cellulose electrospun nanofibers. *Carbohydr Polym* 207:796–805
- Haas D, Heinrich S, Greil P (2010) Solvent control of cellulose acetate nanofibre felt structure produced by electrospinning. *J Mater Sci* 45:1299–1306. <https://doi.org/10.1007/s10853-009-4082-7>
- He H, Fan G, Saba F et al (2023) Enhanced distribution and mechanical properties of high content nanoparticles reinforced metal matrix composite prepared by flake dispersion. *Compos B Eng*. <https://doi.org/10.1016/j.compositesb.2023.110514>
- Higashi S, Hirai T, Matsubara M et al (2020a) Dynamic viscosity recovery of electrospinning solution for stabilizing elongated ultrafine polymer nanofiber by TEMPO-CNF. *Sci Rep*. <https://doi.org/10.1038/s41598-020-69136-2>
- Il BW, Pant HR, Nama KT et al (2011) Effect of adhesive on the morphology and mechanical properties of electrospun fibrous mat of cellulose acetate. *Carbohydr Res* 346:1956–1961. <https://doi.org/10.1016/j.carres.2011.05.025>
- Khoshnevisan K, Maleki H, Samadian H et al (2018) Cellulose acetate electrospun nanofibers for drug delivery systems: applications and recent advances. *Carbohydr Polym* 198:131–141
- Kim ID, Rothschild A, Lee BH et al (2006) Ultrasensitive chemiresistors based on electrospun TiO₂ nanofibers. *Nano Lett* 6:2009–2013. <https://doi.org/10.1021/nl061197h>
- Kumar S, Shandilya M, Uniyal P et al (2023) Efficacy of polymeric nanofibrous membranes for proficient wastewater treatment. *Polym Bull* 80:7145–7200. <https://doi.org/10.1007/s00289-022-04417-6>
- Li WJ, Laurencin CT, Catterson EJ et al (2002) Electrospun nanofibrous structure: a novel scaffold for tissue engineering. *J Biomed Mater Res* 60:613–621. <https://doi.org/10.1002/jbm.10167>
- Li Y, Yao M, Liang C et al (2022) Hemicellulose and nano/microfibrils improving the pliability and hydrophobic properties of cellulose film by interstitial filling and forming micro/nanostructure. *Polymers (basel)*. <https://doi.org/10.3390/polym14071297>
- Liu H, Lo HY (2002) Ultrafine fibrous cellulose membranes from electrospinning of cellulose acetate. *J Polym Sci B Polym Phys* 40:2119–2129. <https://doi.org/10.1002/polb.10261>
- Lu H, Guccini V, Kim H et al (2017) Effects of different manufacturing processes on TEMPO-oxidized carboxylated cellulose nanofiber performance as binder for flexible lithium-ion batteries. *ACS Appl Mater Interfaces* 9:37712–37720. <https://doi.org/10.1021/acsami.7b10307>
- Luo J, Huang K, Xu Y, Fan Y (2019) A comparative study of lignocellulosic nanofibrils isolated from celery using oxalic acid hydrolysis followed by sonication and mechanical fibrillation. *Cellulose* 26:5237–5246. <https://doi.org/10.1007/s10570-019-02454-5>
- Ma Z, Kotaki M, Inai R, Ramakrishna S (2005) Potential of nanofiber matrix as tissue-engineering scaffolds. *Tissue Eng* 11:101–109
- Ma LL, Ye H, Liu L et al (2023) Polypropylene membranes with high adsorption capacity and anti-adhesion properties achieved by hydrophobic interactions and hydrogen bonded self-assembly for uranium extraction from seawater. *Chem Eng J*. <https://doi.org/10.1016/j.cej.2022.138696>
- Morais MS, Bonfim DPF, Aguiar ML, Oliveira WP (2022) Electrospun poly (vinyl alcohol) nanofibrous mat loaded with green propolis extract, chitosan and nystatin as an innovative wound dressing material. *J Pharm Innov*. <https://doi.org/10.1007/s12247-022-09681-7>
- Pavithran R, Reddy MLP, Junior SA et al (2005) Synthesis and luminescent properties of novel europium(III) heterocyclic β -diketone complexes with Lewis bases: structural analysis using the sparkle/AM1 model. *Eur J Inorg Chem*. <https://doi.org/10.1002/ejic.200500461>
- Peng XW, Ren JL, Zhong LX, Sun RC (2011) Nanocomposite films based on xylan-rich hemicelluloses and cellulose nanofibers with enhanced mechanical properties. *Biomacromol* 12:3321–3329. <https://doi.org/10.1021/bm2008795>
- Pino-Ramos VH, Iván Meléndez-Ortiz H, Ramos-Ballesteros A, Bucio E (2017) Radiation grafting of biopolymers and synthetic polymers: synthesis and biomedical applications. In: *Biopolymer grafting: applications*. Elsevier, pp 205–250
- Russo F, Castro-Muñoz R, Santoro S, et al (2022) A review on electrospun membranes for potential air filtration application. *J Environ Chem Eng* 10
- Schnell CN, Inalbon MC, Minari RJ, Mocchiutti P (2023) Use of micro/nano- and nanofibrillated cellulose to improve the mechanical properties and wet performance of xylan/chitosan films: a comparison. *ACS Appl Polym Mater*. <https://doi.org/10.1021/acsapm.3c01141>
- Shanbhag A, Barclay B, Koziara J, Shivanand P (2007) Application of cellulose acetate butyrate-based membrane for

- osmotic drug delivery. *Cellulose* 14:65–71. <https://doi.org/10.1007/s10570-006-9091-y>
- Sharma A, Mandal T, Goswami S (2021) Fabrication of cellulose acetate nanocomposite films with lignocellulosic nanofiber filler for superior effect on thermal, mechanical and optical properties. *Nano-Struct Nano-Objects*. <https://doi.org/10.1016/j.nanoso.2020.100642>
- Singh K, Khanna V, Chaudhary V (2022) Effect of hybrid reinforcements on the mechanical properties of copper nanocomposites. *ECS J Solid State Sci Technol* 11:097001. <https://doi.org/10.1149/2162-8777/ac8bf9>
- Sinha R, Janaswamy S, Prasad A (2020) Enhancing mechanical properties of electrospun cellulose acetate fiber mat upon potassium chloride exposure. *Materialia (oxf)*. <https://doi.org/10.1016/j.mtla.2020.100881>
- Solier YN, Mocchiutti P, Inalbon MC, Zanuttini M (2022) Thermoplastic films based on polyelectrolyte complexes of arabino glucurono-xylan and polyethylenimine. *Macromol Mater Eng*. <https://doi.org/10.1002/mame.202200108>
- Tarrés Q, Oliver-Ortega H, Alcalà M et al (2020) Research on the strengthening advantages on using cellulose nanofibers as polyvinyl alcohol reinforcement. *Polymers (basel)*. <https://doi.org/10.3390/POLYM12040974>
- Thomas RT, Río D, de Vicente JI, Zhang K et al (2022) Size exclusion and affinity-based removal of nanoparticles with electrospun cellulose acetate membranes infused with functionalized cellulose nanocrystals. *Mater Des*. <https://doi.org/10.1016/j.matdes.2022.110654>
- Tripathi A, Ferrer A, Khan SA, Rojas OJ (2017) Morphological and thermochemical changes upon autohydrolysis and microemulsion treatments of coir and empty fruit bunch residual biomass to isolate lignin-rich micro- and nanofibrillar cellulose. *ACS Sustain Chem Eng* 5:2483–2492. <https://doi.org/10.1021/acssuschemeng.6b02838>
- Vatanpour V, Pasaoglu ME, Barzegar H et al (2022) Cellulose acetate in fabrication of polymeric membranes: a review. *Chemosphere* 295:133914
- Vatanpour V, Yuksekdogan A, Ağtaş M et al (2023) Zeolitic imidazolate framework (ZIF-8) modified cellulose acetate NF membranes for potential water treatment application. *Carbohydr Polym*. <https://doi.org/10.1016/j.carbpol.2022.120230>
- Wang B, Kang H, Yang H et al (2019) Preparation and dielectric properties of porous cyanoethyl cellulose membranes. *Cellulose* 26:1261–1275. <https://doi.org/10.1007/s10570-018-2132-5>
- Wongsasulak S, Patapeejumrongsong M, Weiss J et al (2010) Electrospinning of food-grade nanofibers from cellulose acetate and egg albumen blends. *J Food Eng* 98:370–376. <https://doi.org/10.1016/j.jfoodeng.2010.01.014>
- Wsoo MA, Shahir S, Mohd Bohari SP et al (2020) A review on the properties of electrospun cellulose acetate and its application in drug delivery systems: a new perspective. *Carbohydr Res* 491:107978
- Xue J, Wu T, Dai Y, Xia Y (2019) Electrospinning and electrospun nanofibers: methods, materials, and applications. *Chem Rev* 119:5298–5415
- Yan B, Zhang Y, Li Z et al (2022) Electrospun nanofibrous membrane for biomedical application. *SN Appl Sci* 4:172
- Yang S, Ding K, Wang W et al (2022) Electrospun fiber-based high-performance flexible multi-level micro-structured pressure sensor: design, development and modelling. *Chem Eng J*. <https://doi.org/10.1016/j.cej.2021.133700>
- Zhijiang C, Yi X, Haizheng Y et al (2016) Poly(hydroxybutyrate)/cellulose acetate blend nanofiber scaffolds: preparation, characterization and cytocompatibility. *Mater Sci Eng, C* 58:757–767. <https://doi.org/10.1016/j.msec.2015.09.048>
- Zhou Z, Lin W, Wu XF (2016) Electrospinning ultrathin continuous cellulose acetate fibers for high-flux water filtration. *Colloids Surf A Physicochem Eng Asp* 494:21–29. <https://doi.org/10.1016/j.colsurfa.2015.11.074>
- Zou D, Lee YM (2022) Design strategy of poly(vinylidene fluoride) membranes for water treatment. *Prog Polym Sci* 128:101535

Publisher's Note Springer Nature remains neutral with regard to jurisdictional claims in published maps and institutional affiliations.